

Heat transfer with mechanically driven thermal contact resistance at the polymer–mold interface in injection molding of polymers

H. Massé ^a, É. Arquis ^a, D. Delaunay ^{b,*}, S. Quilliet ^c, P.H. Le Bot ^d

^a Laboratoire MASTER-ENSCPB, 16 av. Pey Berland, 33607 Pessac, France

^b Laboratoire de Thermocinétique de l'école Polytechnique de l'université de Nantes, CP 3023, 44087 Nantes cedex 03, France

^c CERAP, 27 bd. Du 11 novembre, 69100 Villeurbanne, France

^d Inergy, 310 rue de Ransbeek, 1120 Brussels, Belgium

Received 3 December 2001; received in revised form 4 April 2002

Abstract

Plastics are materials which show important volume variations when they undergo temperature changes. During the injection molding process, polymer parts may shrink and so become unstuck from the mold walls. It drives then to the apparition of air gaps which may modify both the shape of the part and its cooling time. The cooling of such a polymer part is studied, taking into account key parameters such as thermal contact resistances, residual stresses, or PvT diagram. The results of the numerical simulation, using a coupled thermomechanical approach, are compared to experiments that are led in parallel.

© 2003 Elsevier Ltd. All rights reserved.

1. Introduction

During the cooling of an injected polymer, a very strong coupling exists between the thermal and mechanical phenomena. In order to fill the mold and to compensate the effects of reduction of the volume bound on the thermal shrinkage and possibly on the solidification shrinkage for the semi-crystalline polymers, the pressure in the molding cavity is maintained to a very high level. This is possible if the injection gate that separates the molding cavity of the runners full of polymer is not solidified. As the gate is generally thin to allow the comfortable separation of the piece with the sprue (matter frozen in the feeding channels of the piece), this solidification generally occurs early in the cycle. The decrease of the temperature provokes a shrinkage that leads to the decrease of the pressure in the

molding cavity. It provokes a strong modification of the contact conditions between polymer and mold, and even the apparition of an air gap. The pressure therefore conditions the cooling. When the piece is no more in contact with the mold, its shape, so the thickness of the air gap, is determined by the field of displacement and therefore of stresses in the piece. One conceives then the very strong triangular coupling existing between the temperature, the heat transfer at the interface and the pressure or the stresses in the solid after detachment. The knowledge of the contact resistance is very important for the simulation of the injection process since the temperature of the polymer can be very different from the one of the mold [1], notably at the beginning of cooling when the heat fluxes are very large. The thermal barrier can be important enough, so that in some cases, a local heating of the piece happens, that, if it is not taken into account forbids the calculation of the shrinkage and of the warpage (stress relaxation for example). Several works concern thermal contact resistances between a polymer and a metal. The measurements by classical stationary methods give for

* Corresponding author. Fax: +33-2-40-68-31-41.

E-mail address: didier.delaunay@polytech.univ-nantes.fr (D. Delaunay).

the heat flux through the interface, this one including zones of contact and interstices in which gas is trapped. The main part of the resistance is due to the constriction of the heat flux lines in the zone at the neighborhood of the interface. The statistical analysis of the surface permits to estimate the area and the number of points of contact and acts as basis to models that give satisfactory enough results for metals [11]. This approach is with difficulty transposable to the case of the injection where the polymer surface behavior is difficult to specify and can evolve for example if some slips occur. A difficulty is also linked to the transient character of the process. In the beginning of the filling, at the time of the abrupt contact, one must consider the setting time of the constriction resistance. It is possible to estimate it by $\tau = 100r^2/a$, where r is the surface of contact radius and a the weighted diffusivity of the two contacting bodies. The order of magnitude is the millisecond. One can consider therefore that the resistances are established. Their expression leads to determine the surface temperatures of the mold $T_{ms}(t)$ and of the polymer $T_{ps}(t)$, as well as the flux $\Phi(t)$ which crosses the interface:

$$R(t) = (T_{ms}(t) - T_{ps}(t))/\Phi(t) \quad (1)$$

The measurement of the surface temperature of the mold and of the heat flux that crosses the interface is relatively comfortable, notably by inverse method to go back to the surface. This method is impossible to use for the polymer, in which one cannot introduce any sufficiently thin sensors so that they do not modify the temperature field. The method that we used as well as its validation is described in the Ref. [1]. We chose an indirect method that consists in calculating the temperature field in the thickness of the injected plate, while supposing that the transfers are 1D in this one, and while using the experimental heat flux evolutions versus the time as boundaries conditions. From the moment the initial temperature field is known, this calculation is possible if the thermal properties, and notably their variation according to the temperature is known. In the case of an amorphous polymer, it does not pose any particular problem. In the case of a semi-crystalline polymer, the source released at the crystallization is not known with precision in fast cooling, which is the case at the beginning of the solidification during injection. The kinetic effects prevent to determine the contact resistance precisely then, at least during the first instants. It is the reason why we used the ABS which is an amorphous polymer. The specific heat has been determined by using a differential scanning calorimeter, in cooling mode, at 8 K/min. The PVT diagrams have been measured by using a SWO PVT100 device. The thermal conductivity has been measured using the device and the method described in Ref. [12]. The values of these parameters and their variations with the temperature are indicated in Fig. 1a–c.

As we already underlined it, the initial temperature field is necessary to compute the thermal contact resistance. Two different methods have been used, that gave very close results. The first one consisted in using a software to simulate the filling of the mold. The second one, described in the Ref. [1], consisted to use an inverse method to go back to the initial state. A multiple criteria method based on the variation of the heat fluxes on the faces of the sample as well as on the integral of this one has been used. Indeed, the initial temperature distribution cannot be gotten in an unique manner if one uses only the heat fluxes. On the other hand, if one knows the final enthalpy, by adding a criteria on the integral of these fluxes, the solution becomes unique. Fig. 2 shows an example of temperature field identified in the thickness of the molding cavity, at the end of the filling. We also show the field calculated at the same instant by the software Moldflow®. The profiles are very close.

A mold made of steel (40 CMD8) molding plates of $0.012 \text{ m} \times 0.014 \text{ m} \times 0.002 \text{ m}$ has been used. On each of the two faces, in the center of the plate, two heat flux and surface temperature sensors are placed one in front of the other. A pressure sensor is placed close to these thermal sensors. We have verified by simulation that the surfaces of the molding cavity had an uniform temperature. The maximal temperature gap at the end of filling is of the order of 1 K. The transfers are therefore well 1D in the thickness.

The heat flux and mold surface temperature sensors whose schematic views are shown in Fig. 3a and b are composed of a cylindrical measurement cell, Fig. 3b, lodged in a body, Fig. 3a. The cell is composed of two half cylinders whose plan of cut is perpendicular to the molding cavity surface, in order not to modify the flux. For the same reason, the metal of the sensor and its surface roughness are identical to the one of the mold. The simulation of the thermal behavior of the sensor in the mold has been done, to verify that the flux that crosses it is well identical to the one that exists in its absence. One shows that up to a distance of 5 mm of the surface, the temperature field is not disrupted and remains one-dimensional well. Three thermocouples of 12 μm diameter are placed along the isotherms, that is to say parallel to the surface (Fig. 4). They are intrinsic thermocouples since the extremities of the chromel and alumel wires are welded on the body of the sensor and separated by a portion of isothermal metal. The part of the junction in the metallic body of the sensor does not intervene therefore in the measurement but participates to improve the response of the sensor. Their position in relation to the surface is fixed according to the rules of the inverse method used to exploit the measurements. The first one consists in placing the thermocouple that will act as boundary condition as far as possible of the surface, in the zone where the transfers remain 1D. It is placed therefore at 5 mm. The thermocouple closer to

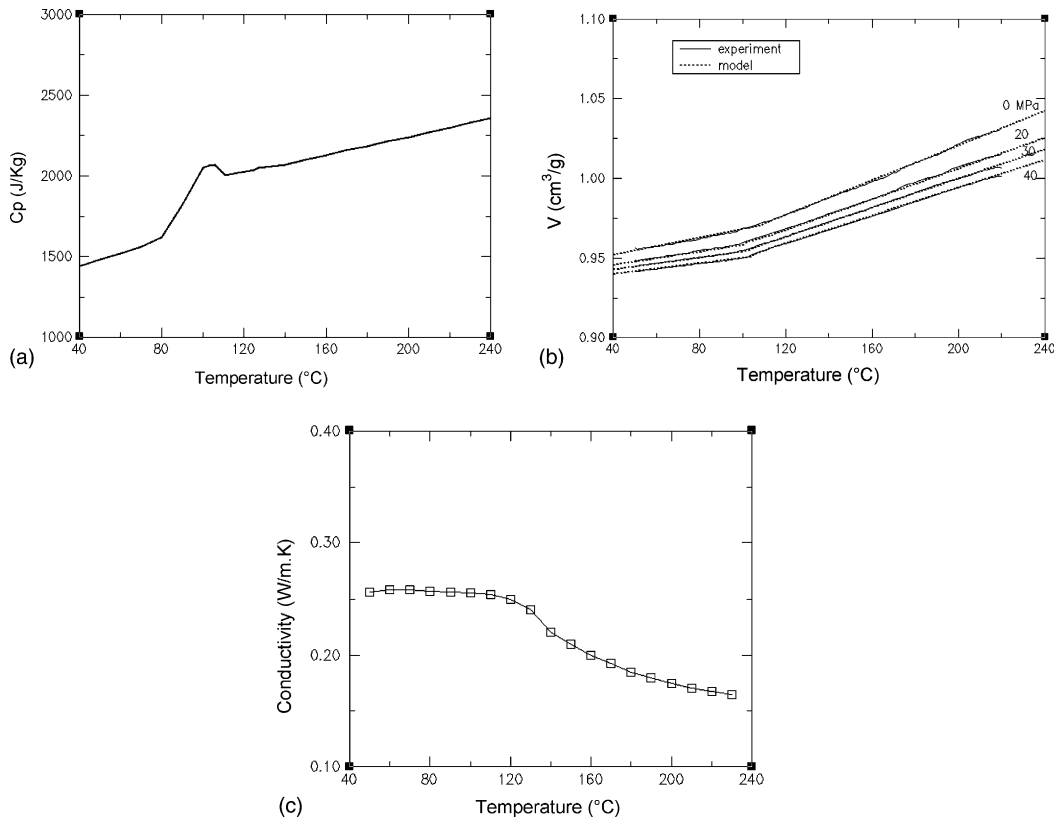


Fig. 1. Thermal properties of ABS: (a) specific heat, (b) PvT diagram, (c) thermal conductivity.

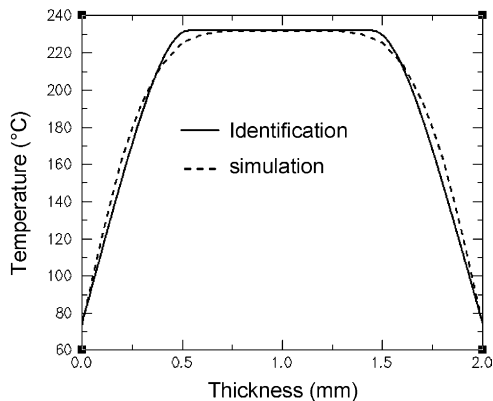


Fig. 2. Initial temperature field in the piece identified by inverse method and calculated by Moldflow.

the molding cavity is placed as close as the surface as possible in regard of the technical constraints. It is so at a depth of 200 μm . An intermediate thermocouple is placed at a distance of 2 mm, in order to calculate the residues. Its sensitivity in term of heat flux determination is weaker than for the one placed closer to the surface.

The wires of the thermocouples are connected to a reference box in which a platinum probe is placed. Amplified tension is recorded then by a rapid data acquisition system, at a frequency of 1 ms. A classical sequential method [13] is used to get flux and surface temperature. The good work of the sensors is verified on a special apparatus described in detail in the Ref. [9]. A characteristic example of flux and surface temperature is shown in Fig. 5a and b. At the time of the contact of the hot polymer, the temperature increases suddenly. If there were no contact resistance, the contact temperature would be reached instantaneously. In presence of this one, the increase rate is limited. The temperature decreases then, with the progression of the cooling of the piece. At the time of contact heat flux is theoretically infinite, it reached $10^5 \text{ W/m}^2 \text{ s}$ at the end of the filling, decreases then to become equal to zero when the piece is cooled.

Fig. 6 shows the evolution of the thermal contact resistance, for a cycle corresponding to the evolution of pressure indicated on this figure, using the right hand scale. The initial time $t = 0 \text{ s}$ corresponds to the end of the filling. The pressure decreases in the molding cavity, because of the frost of the gate that is almost immediate.

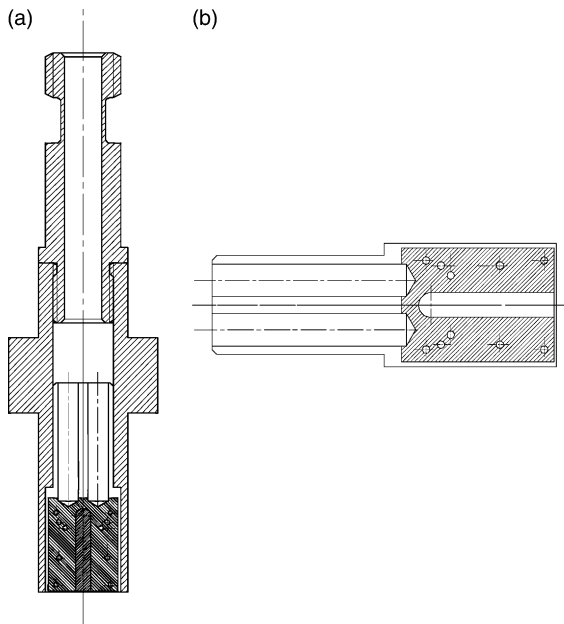


Fig. 3. Technical scheme of the heat flux and mold surface temperature sensor: (a) a cut of the body of the sensor. Inside this one, a cylindrical measurement cell is lodged, (b) a view of one of the two half-cylinders which constitute this cell, for which a detail is shown in Fig. 4.

The contact resistances that are equal on the two faces of the piece increase as the pressure decreases. One sees that they double between the beginning and the end of the cooling phase where the piece is in contact with the mold. Their mean values are of $5 \times 10^{-4} \text{ m}^2 \text{ K W}^{-1}$, which is in conformity with the values observed by Yu et al. [5]. When the pressure becomes equal to the atmospheric pressure, the resistances increase brutally while remaining equal on the two opposed faces of the cavity. In this case, the air gap distributes itself in an identical manner on the two faces of the sample.

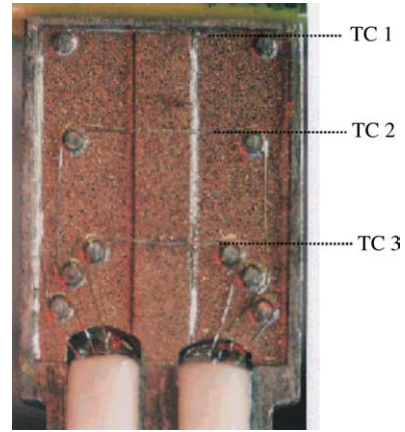


Fig. 4. View of the sensor showing the thermocouples wires along the isotherm.

We show in Fig. 7 the results that we get for different molding cavity surfaces. The results for three different roughness ($Ra = 0.05 \mu\text{m}$, $Ra = 1 \mu\text{m}$, $Ra = 5 \mu\text{m}$) are presented as well as for a surface of roughness $Ra = 1 \mu\text{m}$ covered with chromium or Teflon. The drawn curves are obtained showing in abscissa the instantaneous value of the pressure. For every surface, a logarithmic evolution of the conductance according to the pressure is noticed. The chromium-plating does not modify the contact resistance whereas the coating of Teflon decreases the conductance, which was foreseeable. Having some results for three different roughness, it was interesting to examine the evolution of the conductance according to the roughness, for different values of the instantaneous pressure. One notes that the conductance decreases when the roughness increases. The quantity of air captured between the peaks of the surface explains this evolution. Although only three values are available, one gets nevertheless a linear evolution of the conductance according

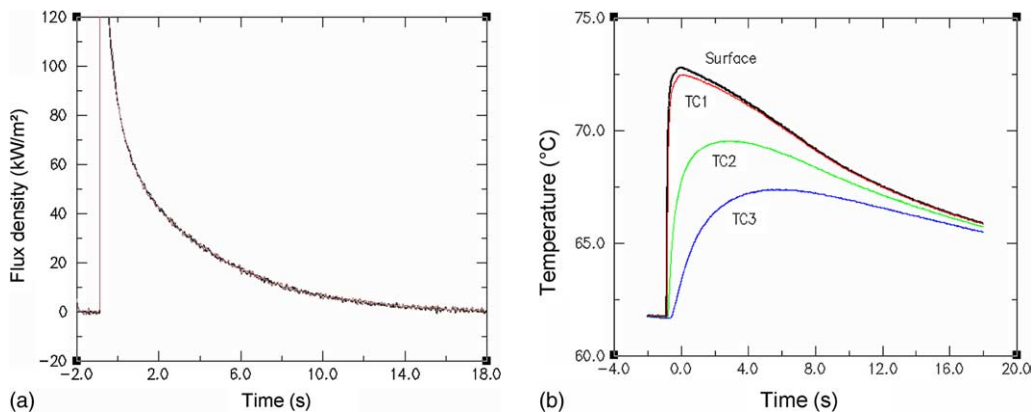


Fig. 5. Example of measure of heat flux and surface temperature of the mold. (a) heat flux, (b) mold temperature.

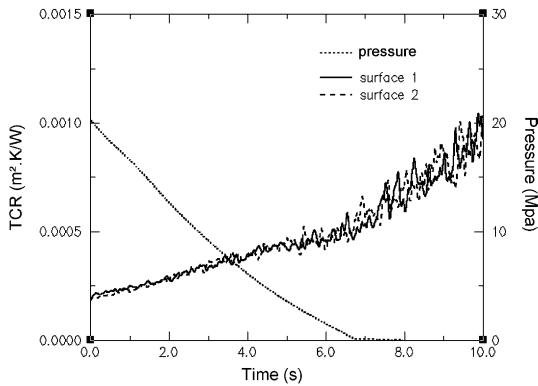


Fig. 6. Evolution of the thermal resistances at the polymer–mold interface.

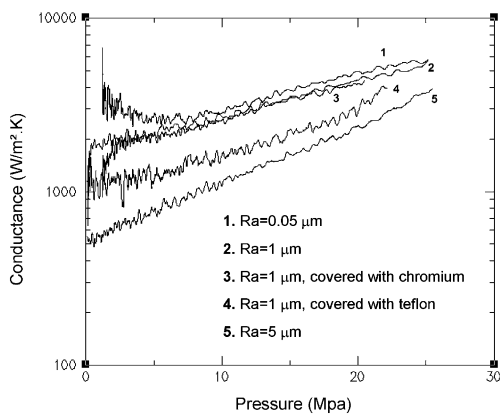


Fig. 7. Evolution of the conductance according to the pressure. Influence of the roughness of the mold.

to the roughness. One proposes the empiric law (2) to calculate the contact resistance between the surface of the mold and of the polymer

$$R(t) = R_0 \exp(-(P(t)/P_0)) \quad (2)$$

R_0 and P_0 are constants that depend on the roughness of the mold. For confidentiality reasons, their exact values cannot be given here. This result is only valid for a couple of mold–polymer material, the resistance also depending, but of secondary manner of the conductivity of the materials in contact. Indeed, the role of the interstitial gas is not negligible in relation to the passage by the points of contact. Its decompression during the cooling and therefore the variation of its volume strongly modifies the conditions of contact and forbid the use of classical models. A thermomechanical analysis at a microscopic scale would be necessary to go further in the modeling.

3. Modeling of the cooling phase

3.1. General presentation

The simulation uses the finite volumes method. The equations are written in a conservative form, which makes finite volumes a natural method to solve the equations of the fluids mechanics of the and the heat transfers [14].

Traditionally, the equations of the solid mechanics are solved by finite elements methods. Some authors begin however to use the finite volumes to solve these equations in particular I. Demirdzic [15,16]. Hattel [17] uses also a technique of finite differences.

One applies the small perturbation hypothesis (small displacements, small strains, small temperature variations), that supposes that the displacements between two time steps in the solid material are sufficiently small. The position of the nodes of the mesh remains unaltered during the calculation, but a displacement of these nodes is calculated during the time.

3.2. Formulation of the equations

At the end of the filling phase, the piece cools and solidifies in the mold. The physical phenomena are piloted then by the state equation of the polymer, the displacements equation and the energy equation.

3.2.1. State equation

The specific volume joins the variations of temperature and pressure to the volume of the material through the PvT diagram. This relation designed as state equation may be written in the general form

$$f(P, v, T) = 0 \quad (3)$$

Although theoretical approaches of this state equation exist, it is generally represented by an empirical model based on the measurements. We chose the Tait relation [18], currently used in the literature [19], that gives a good approximation of the PvT diagram and whose coefficients have been tabulated for many polymers. This relation is

$$\frac{v(0, \tilde{T}) - v(p, \tilde{T})}{v(0, \tilde{T})} = C \ln \left(1 + \frac{p}{B(\tilde{T})} \right) \quad (4)$$

Where the variation of $T_g = f(p)$ is linear, its evolution being deduced from experimental results

$$T_g(p) = T_g(0) + \frac{0.55}{3} p \quad (5)$$

One notes that the use of this relation requires the knowledge of three parameters:

- the specific volume at atmospheric pressure $v(0, T)$,
- the adimensional constant C ,
- the function $B(T)$, that has the dimension of a pressure.

Simha et al. [20] showed that C is nearly constant (better approximation: $C = 0.0894$) and that $B(T)$ can be written

$$B(T) = b_1 e^{-b_2 T} \tag{6}$$

The constant b_2 has a mean value of 4.5×10^{-3} while b_1 depends on the nature of the polymer, but is proportional to the elastic module of compression $K = \frac{E}{3(1-2\nu)}$. We use $b_1 = 3.3 \times 10^{-2}$ K, which permits to approach the measurements satisfactorily (Fig. 1b).

The knowledge of the PvT diagram of the material permits us, if we consider that the material has a quasi elastic behavior, to deduce the values of the density and of thermal expansion coefficient, which depend at a time on the temperature and the pressure

$$\rho = \frac{1}{v}; \quad \alpha = \frac{1}{v} \left(\frac{\partial v}{\partial T} \right)_p; \quad \beta = \frac{\alpha E}{1 - 2\nu} \tag{7}$$

The use of this last equation includes some limitations however. Indeed, even though it is possible to give a realistic enough evolution of the Poisson’s coefficient (for example $\nu = 0.2$ for $T < T_g$ and $\nu = 0.4$ for $T > T_g$), the detachment of the piece makes it the bulk modulus unrealistic when the pressure at the surface of the piece becomes equal to the atmospheric one. It is then necessary to use the measured values of the Young modulus, in the relation giving the variation of the bulk modulus.

3.2.2. Displacements equation

The unknown of this equation are the components of the displacements vector. In the formulation that we propose, it is the equilibrium equation that is written and that allows to obtain the discrete displacements equation (on an irregular Cartesian mesh) following the way presented in Fig. 8.

The static equation of equilibrium is

$$\frac{1}{V} \int \int \int_D \nabla \cdot \bar{\sigma} dv = 0 \tag{8}$$

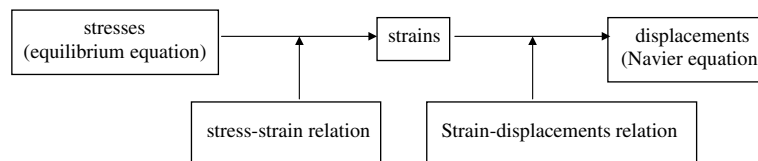


Fig. 8. Displacement equation from equilibrium equation.

While using the theorem of the divergence, we obtain

$$\frac{1}{V} \int \int \int_S \bar{\sigma} \cdot \bar{n} ds = 0 \tag{9}$$

The elastic behavior leads to write the stress tensor

$$\bar{\sigma} = \lambda(\text{tr} \bar{\epsilon}) \bar{I} + 2\mu \bar{\epsilon} - \beta \tau \bar{I} \tag{10}$$

The equation that links the deformation to the displacements is then used

$$\bar{\epsilon} = \frac{1}{2} (\nabla U + \nabla^T U) \tag{11}$$

We get the displacements (or Navier) equation

$$\nabla(\lambda \nabla \cdot U) + \nabla \cdot [\mu(\nabla U + \nabla U^T)] - \nabla(\beta \tau) = 0 \tag{12}$$

The discrete form on the Cartesian volume presented in Fig. 9 gives

$$\begin{cases} \frac{1}{dx dy} \int \int_S [\sigma_{xx}(e) - \sigma_{xx}(w)] dy \\ + \frac{1}{dx dy} \int \int_S [\sigma_{xy}(n) - \sigma_{xy}(S)] dx = 0 \\ \frac{1}{dx dy} \int \int_S [\sigma_{xy}(e) - \sigma_{xy}(w)] dy \\ + \frac{1}{dx dy} \int \int_S [\sigma_{yy}(n) - \sigma_{yy}(S)] dx = 0 \end{cases} \tag{13}$$

where e , w , n and s are the respective indications of the east, west, south and north faces of a control volume.

The derivatives of the displacements vector U components are approached by a finite differences scheme. While noticing that the main term derivatives (u or v for the equation projected respectively according to x or y) are in the direction normal to the surfaces on which they are defined, we use a five points discrete scheme. By example

$$\frac{\partial b^n}{\partial x}(e) = \frac{\partial b^s}{\partial x}(e) = \frac{b_{i+1,j} - b_{i,j}}{\Delta x_e} \quad b = u, v \tag{14}$$

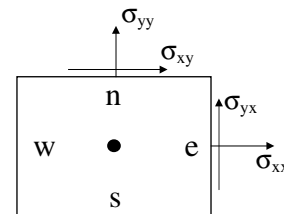


Fig. 9. Control volume for the discrete equations.

The terms of coupling u (respectively v) for the equation projected according to x (respectively y) have their derivatives in a tangent direction to the surface on which they are defined. We use then a nine points discrete scheme. By example

$$\frac{\partial b^w}{\partial y}(s) = \frac{(b_{i,j} + b_{i-1,j}) - (b_{i,j-1} + b_{i-1,j-1})}{2\Delta y_s} \quad b = v, u \quad (15)$$

We get a matrix system then where the main blocks A and D contain five diagonals, while the coupling blocks B and C contain nine diagonals

$$\begin{bmatrix} A & B \\ C & D \end{bmatrix} \begin{bmatrix} U \\ V \end{bmatrix} = \begin{bmatrix} \phi_x \\ \phi_y \end{bmatrix} \quad (16)$$

3.2.3. Energy equation

In the packing phase and after freezing of the gate, the shear rate is very small and viscous dissipation is negligible. So, the equation of the energy may be written in the form of

$$\frac{1}{v} C_p(T) \frac{\partial T}{\partial t} - \alpha(T, p) T \frac{\partial p}{\partial t} = \nabla \cdot (k(T) \nabla T) \quad (17)$$

We have already noted the strong influence of the resistances on the evolution of the temperature field. Besides the contact resistance that has been quantified in the previous paragraph, a thermal resistance exists due to the air gap that can come in between the piece and the mold during the cooling. It is therefore necessary to know the displacements and the deformation of the piece to calculate this thermal resistance correctly.

At the time of the detachment, that is to say when the stress at the polymer–mold interface becomes equal to the atmospheric pressure, an initial thickness of the air gap equal to the value of the contact resistance at this instant ($t = 7$ s in Fig. 6) is considered. The interface conductance expresses then

$$h(t) = \frac{1}{\frac{\delta}{R_{\text{air}}} + R(p(t))} \quad (18)$$

Thermal conductivity and specific heat have been measured at the laboratory and have been used in the simulation. The density comes from the PvT diagram and depends therefore on the pressure and the temperature.

3.3. Discrete equations

The state, displacements and energy equations are written in discrete form in space and time, by using the control volume represented in Fig. 9.

For the energy equation a classic Quick scheme is used. The algorithm consists in solving in a first step the

energy equation, then the state equation gives $v(t^n, p^{n-1})$. One can calculate then $\alpha(t^n, p^{n-1})$ as well as $\beta(t^n, p^{n-1})$ what permits to solve the displacements equation. The deformations are then calculated and the resolution of Eq. (10) gives the stresses and therefore the new pressure.

In theory iterations on the pressure are necessary but we noticed that they do not bring a considerable modification to the result for very small time steps (10^{-3} s).

4. Presentation of the results and comparison to the experiments

We present here two results. The first one corresponds to a packing pressure of 40 MPa, the temperature mold regulation being programmed in order to ensure a good thermal symmetry all along the experience. It corresponds to a mold different of the one used to determine the relations giving the thermal contact resistance, but it is constituted of the same material and has the same surface roughness. It permits to achieve square pieces of $0.062 \text{ m} \times 0.062 \text{ m}$ and of 3 mm thickness. The flux and surface temperature sensors are arranged on the two large faces of the piece, as indicated in Fig. 10.

We present the result of surface temperature recorded by one of the thermal sensors in Fig. 11. On this graph are presented the data obtained by the three thermocouples constituting the sensor and the surface temperature identified, which is nearly confounded with the data coming from the thermocouple closer to the surface.

The acquisition time includes three cycles (filling, packing, cooling, ejection). A very good reproducibility of the temperatures of a cycle on the other is noticed, what shows that the press reached its thermal balance when the measurements have been done.

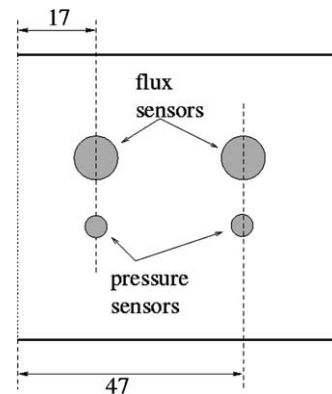


Fig. 10. Position of the temperature and pressure sensors on the surface of the molding cavity.

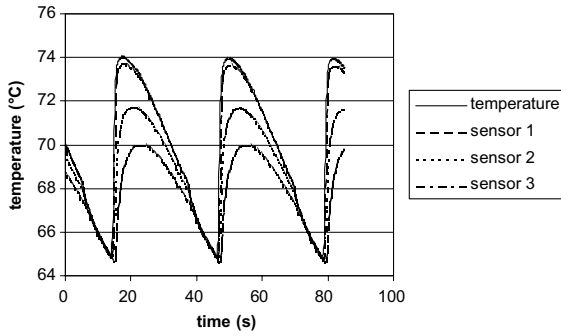


Fig. 11. Heat flux sensor measurements (three thermocouples and the identified temperature).

The surface temperatures being nearly confounded for the two sensors situated in front one of the other, only one is shown. One also notes the instant of the ejection, 16 s after the injection, the evolution of the surface temperature showing an angular point.

We used the plans of the mold to reproduce the position as well as the size of the cooling channels. The heat fluxes extracted by these channels are estimated according to the temperature of the cooling water, that can be considered constant with a 0.1 K precision. The heat transfer coefficient between the cooling water and the channel is computed by a classical correlation [21]. The other conditions at the boundaries of the calculation domain have been calculated taking into account the mold thermal resistance.

The coupled calculation of heat transfer and mechanics starts at the end of the filling. The initial temperature profile is simulated by the cooling of a polymer initially to uniform temperature equals to 235

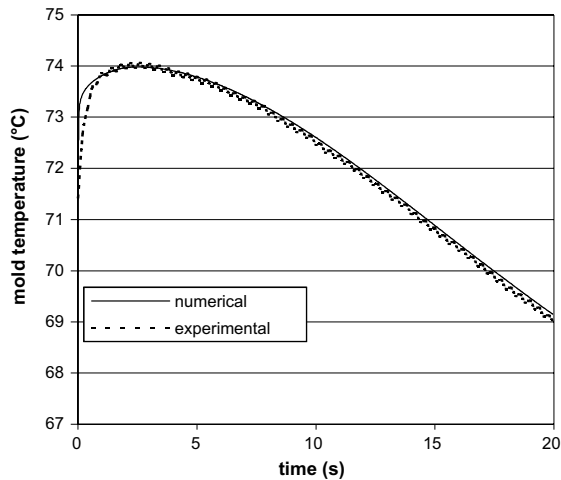


Fig. 12. Comparison between measure and simulation: temperature of the mold.

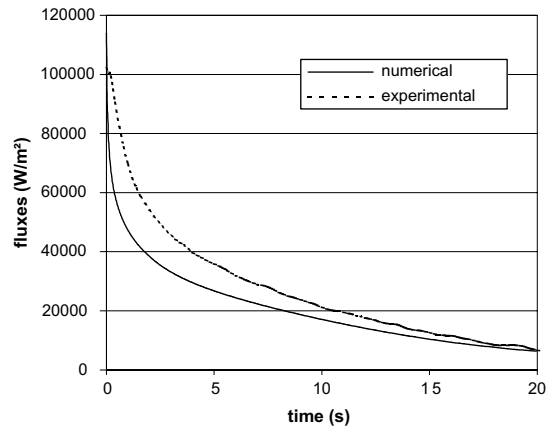


Fig. 13. Comparison between measure and simulation: heat flux at the interface.

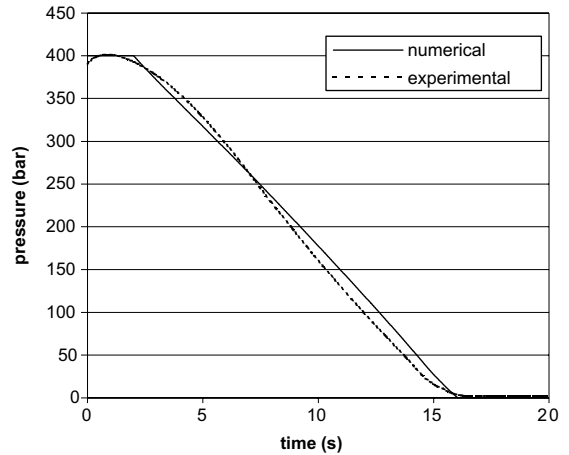


Fig. 14. Comparison between measure and simulation: pressure at the interface.

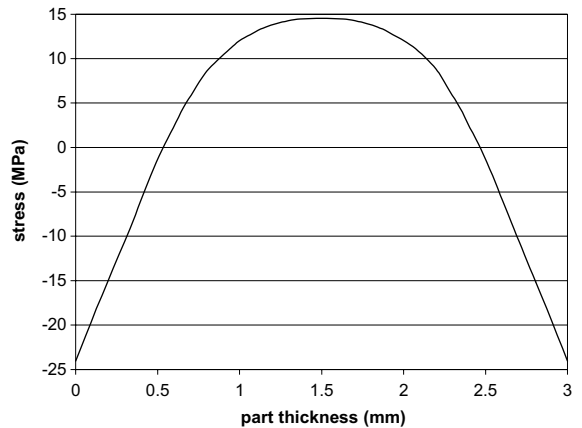


Fig. 15. Residual stresses trapped in the thickness of the piece after cooling.

°C put in contact with a mold to 60 °C. The beginning of the calculation corresponds to 0.45 s after the contact time.

The calculations are done on a Cray J90 with 200 Mflops by processor power. The modeling of a 20 s. cycle requires about 72 h of CPU time.

Figs. 12–14 show the comparison between the measurements and the calculation of the mold temperatures, of the parietal heat fluxes and of the pressure.

The calculated and measured temperatures at the surface of the mold are in very good agreement. It is also the case for the pressure. This one is imposed at 40 Mpa during 3 s then decreases freely, the gate being supposed frozen at this instant. The moment when the value of the pressure reaches the atmospheric pressure is well predicted, what shows that the evaluation of the variation of the Young modulus is correct. The calculated heat flux is lower than the measured one. We interpret this difference by the fact that we did not take in account the entry of hot polymer during the packing phase. Indeed, if the calculation makes really vary the mass during the cooling under constant pressure, it affects to the entering matter the local temperature during cooling. This creates an internal energy deficit that explains the flux differences.

Fig. 15 shows the residual stresses distribution at the time of the ejection of the piece. This result is quite similar to the results obtained by Struik [22] for an elastic material. The shrinkage being small, one does not note detachment of the piece.

The second example corresponds to a non symmetrical case where a 10 K difference is imposed on the two

faces of a 2 mm thickness piece. The packing has been voluntarily limited to 2.6 Mpa in order to provoke detachment. Fig. 16 shows the evolution of the surface temperature of the polymer calculated by the technique described in the Section 2, in one interval of time where the detachment of the piece occurs. When it occurs, at different times on the two faces of the piece, the surface temperature of this one increases (up to 12 K in this example). This heating is due to the brutal increase of the polymer–mold interface resistance. One observes the effect of a beating of the piece that, at $t = 4.5$ s finds a new position in the axis of the cavity, to come closer of the cold side.

The simulation of this case is shown in Fig. 17. The detachment is observed, as well as the temperature in-

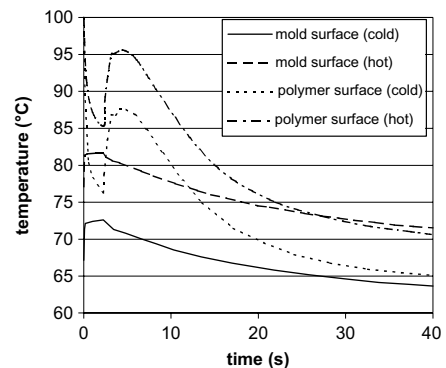


Fig. 17. Calculated evolution of the mold and polymer surface temperatures.

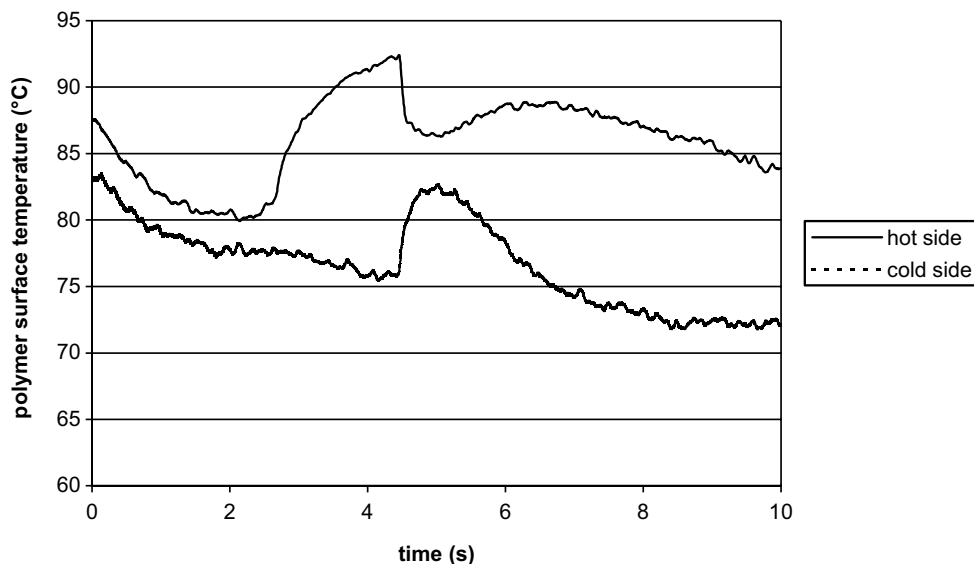


Fig. 16. Experimental polymer surface temperature deduced from inverse analysis. One notes the effect on these temperatures of the air gap occurring in the process.

crease of the polymer. The amplitude of this increase is correctly predicted. The two faces become unstuck in a simultaneous manner, but for surface temperatures close to those observed experimentally. The beating is not put in evidence but the sum of the resistances is compliant to the experimental results. Their evolution is also compliant to the results of Yu et al. [5]. The curve of the calculated evolution of the thermal contact resistances on the two faces is shown in Fig. 18. The sum of the resistances corresponds well to the shrinkage calculated thanks to the PvT diagram. The phenomenon of beating does not seem due in this case to the non uniform stress field in the thickness of the piece, but to the adherence of the piece on the side opposed to the ejectors, by suction effect, caused by the decompression of air trapped in the roughness of the surface of the mold. This suction effect could be simulated by a normal negative additive stress applied to the surface of the piece.

The air gap distribution on the two faces of the piece and its evolution during time is shown in Fig. 19. One observes that shape and amplitude of the air gap on the two faces are not symmetrical. Before 10 s the distribution is identical on each of the two faces. Thereafter, the piece takes a profile of “S”, while coming closer of the cold wall. At the same instant on one face

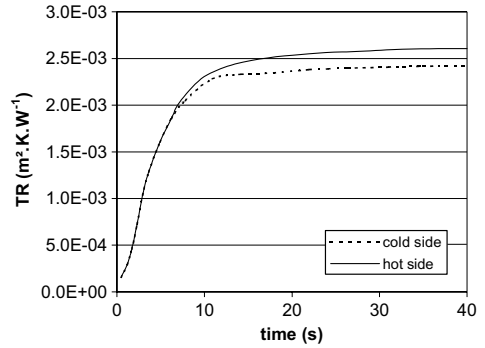


Fig. 18. Evolution of the thermal contact resistances on the faces of the piece.

of the sample the resistances defer 30%, what corresponds to 7 K temperature difference. An interesting result must be noted: the bottom of the piece, solidified just at the end of the filling, does not contract itself in thickness but displaces up of 2 mm, drawn by the shrinkage of the rest of the piece. One can therefore expect important variations of specific volume. In the upper part of the cavity, the gate blocks the shrinkage.

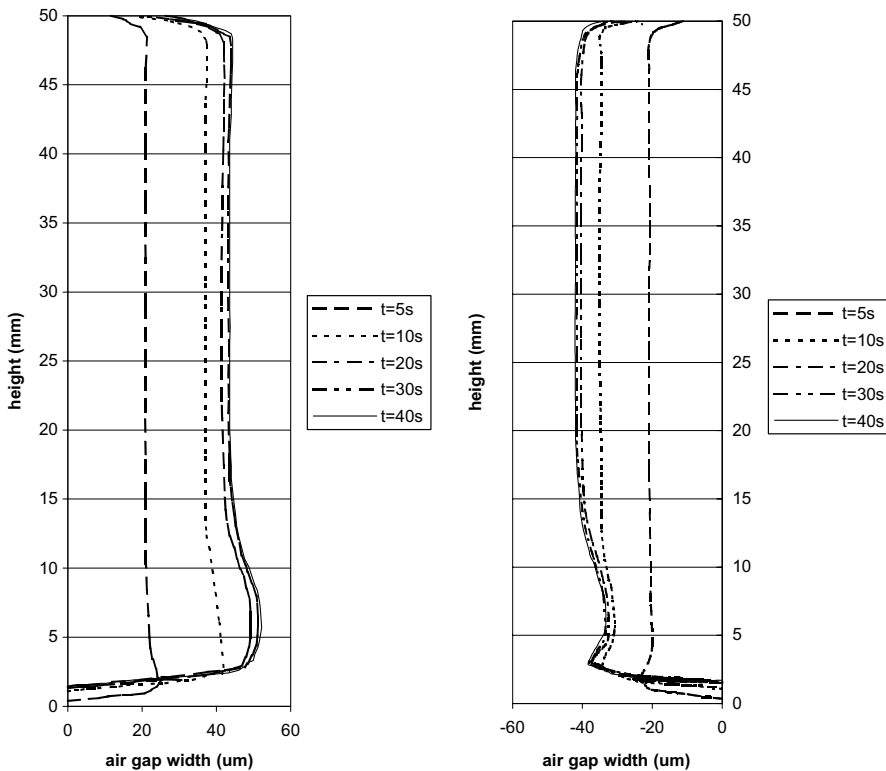


Fig. 19. Distribution of the air gap on the faces of the piece at different times.

5. Conclusion

In a first part, we presented a method to measure the evolution of the thermal contact resistances between an injected polymer and the mold. We propose a relation that permits to predict the time evolution of this resistance for a couple of mold material and polymer and a given roughness. This relation is valid when the piece is in contact with the mold, before the apparition of the air gap due to shrinkage. The classical approaches based on the mechanics of the contact do not allow to get orders of magnitude and evolutions of the resistances in agreement with this empirical relation. Theoretical investigation to interpret this empirical relation constitutes an open field that would permit to better predict these resistances. In the present state, only heavy campaigns of measurements permit to evaluate the R_0 and P_0 coefficients of the model.

In a second part, we present the simulation of the very strong thermal and mechanical coupling during the cooling of a piece in the molding cavity. The calculation is based on simple hypotheses from a mechanical point of view since it supposes an elastic material whose Young modulus and Poisson's coefficient are temperature dependent. The contact resistance depends on the normal stress at the polymer–mold interface according to the previously established empirical relation. After the detachment, the thickness of the air gap is determined by the position of the piece in the mold resulting of the stress distribution due to the temperature field. This model compared to the measurements on a mold different of the one used in the first part permits to obtain a good agreement with the experimental evolutions of mold temperature and of pressure in the molding cavity, and gives a correct behavior for the residual stresses.

In a case of strong shrinkage (no packing) with temperature differences between the surfaces of the molding cavity, the detachment of the piece and the temperature increase on its surface are observed. The time evolutions of resistances are compliant to the experiments both in the evolutions and in the reached values. The effects of gas trapped in the interstices of the mold roughness are important, notably on the apparition of beatings. [9] showed also that the decompression of this interstitial gas permits to interpret the time variation of the contact resistance. The surface temperatures show heterogeneity superior to 5 K. The shape of the piece can be very complex and our results confirm the importance of a thermal and mechanical coupled simulation to foresee the cooling, the shrinkage, and the residual stresses correctly in an injected piece.

The results presented here concern an amorphous material and they are not transposable to a semi-crystalline material. The shrinkages are very important and the relation between pressure and resistance does not seem to be as simple as in the studied case.

Acknowledgements

This work has taken place in the frame of the research network AmETH (“Amélioration des Echanges Thermiques”—Improvement of Thermal Exchange) supported by both the French Ministry of Education and Technological Research, MENRT, and the National Center for Scientific Research, CNRS, SPI Department).

References

- [1] D. Delaunay, Ph. Le Bot, R. Fulchiron, J.F. Luyé, G. Regnier, Nature of contact between polymer and mold in injection molding. Part 1: Influence of a non-perfect thermal contact, *Polym. Eng. Sci.* 40 (7) (2000).
- [2] O. Rhee, Thermal contact measurement, Technical report 80, Cornell Injection Molding Report, 1994.
- [3] J.A. Hall, W.H. Ceckler, E.V. Thomson, Thermal properties of rigid polymers, I. Measurement of thermal conductivity and question concerning contact resistance, *J. Appl. Polym. Sci.* 33 (1987) 2029–2039.
- [4] S.K. Parihar, N.T. Wright, Thermal contact resistances at elastomer to metal interfaces, *Int. Commun. Heat Mass Transfer* 24 (8) (1997) 1083–1092.
- [5] C.J. Yu, J.E. Sunderland, C. Poli, Thermal contact resistance in injection molding, *Polym. Eng. Sci.* 30 (1990) 1599–1605.
- [6] S. Quilliet, Ph. Le Bot, D. Delaunay, Y. Jarny, Heat transfer at the polymer–metal interface: a method of analysis and its application to injection molding, in: *ASME Proceedings of the 32nd National Heat Transfer Conference*, HTD-340, vol. 2, 1997, pp. 9–16.
- [7] L. Shridar, W. Yin, K.A. Narh, The effect of shrinkage induced interface gap on the thermal contact resistance between the mold and plastic in injection molding, *J. Inject. Mold. Tech.* 4 (1) (2000).
- [8] Ph. Le Bot, Comportement thermique des semis-cristallins injectés, Application à la prédiction des retraites, Thèse de Doctorat, Université de Nantes, 1998.
- [9] S. Quilliet, Transferts thermiques à l'interface polymère-métal dans le procédé d'injection des thermoplastiques, Thèse de Doctorat, Université de Nantes, 1998.
- [10] H. Massé, Couplage thermomécanique lors de la solidification de matériaux polymères, Thèse de Doctorat, Université de Bordeaux 1, 2000.
- [11] J.J. Salgon, F. Robe-Valloire, J. Blouet, J. Bransier, A mechanical and geometrical approach to thermal contact resistance, *Int. J. Heat Mass Transfer* 40 (1997) 1121.
- [12] T. Jurkowski, Y. Jarny, D. Delaunay, Estimation of thermal conductivity of thermoplastics under moulding conditions: an apparatus and an inverse algorithm, *Int. J. Heat Mass Transfer* 40 (17) (1997) 4169–4181.
- [13] J.V. Beck, B. Blackwell, C. St. Clair, *Inverse Heat Conduction*, Wiley-Interscience, 1985.
- [14] S.V. Patankar, *Numerical Heat Transfer and Fluid Flow*, Hemisphere, 1990.
- [15] I. Demirdžić, D. Martinović, Finite volume method for thermo-elasto-plastic stress analysis, *Comput. Methods Appl. Mech. Eng.* 109 (1993) 331–349.

- [16] I. Demirdžić, S. Muzaferija, Finite volume method for stress analysis in complex domains, *Comput. Methods Appl. Mech. Eng.* 37 (1994) 3751–3766.
- [17] J.H. Hattel, A control volume-based finite difference method for solving the equilibrium equations in terms of displacements, *Appl. Math. Modell.* 19 (1995) 210–243.
- [18] P.G. Tait, *Phys. Chem.* 2 (1) (1888).
- [19] D.W. Van Krevelen, *Properties of Polymers*, Elsevier, 1990.
- [20] R. Simha, P.S.S. Wilson, O. Olabisi, *Kolloid-Z* 2 (1973) 402.
- [21] W.M. Kays, M.E. Crawford, *Convective Heat and Mass Transfer*, McGraw-Hill, 1993.
- [22] L.C.E. Struik, Orientation effects and cooling stresses in amorphous polymers, *Polym. Eng. Sci.* 18 (10) (1978) 811–817.